First Observations of the New MEXART's Digital System

J. A. Gonzalez-Esparza[1], J.C. Mejia-Ambriz[1,2], E. Aguilar-Rodriguez[1], P. Villanueva[1], E. Andrade[1], A. Magro[3], R. Chiello[4], D. Cutajar[3], J. Borg[3], and K. Zarb-Adami[3,4]

————

Corresponding author: J.A. González-Esparza, LANCE, Instituto de Geofísica, Unidad Michoacán, Universidad Nacional Autónoma de México, Morelia, Michoacán, México. CP 58190. (americo@igeofisica.unam.mx)

[1]LANCE, Instituto de Geofísica, Unidad Michoacán, Universidad Nacional Autónoma de México, Morelia, Michoacán, México. CP 58190.

[2]CONACyT Research Fellow – Instituto de Geofísica, Unidad Michoacán, Universidad Nacional Autónoma de México, Morelia, Michoacán, México. CP 58190.

[3]Institute of Space Sciences and Astronomy, University of Malta, Malta.

June 3, 2021, 6:55pm

Abstract: The Mexican Array Radio Telescope (MEXART) is a transit instrument mainly dedicated to performing Interplanetary Scintillation (IPS) observations with a central operating frequency of 139.65 MHz. The main scientific objective is to perform studies of solar wind properties and space weather effects. MEXART initially operated with an analog beamformer (16x16 Butler matrix), which produced 16 fixed latitudinal beams. MEXART began operations and reported the first measurements of IPS sources. MEXART's beamforming system had several problems, however. The North-South beams had poor directivity, with large side lobes, and the instrument did not achieve the expected performance. Therefore, we commissioned the design and construction of a digital back-end. The digital system solved the problems with the beamforming, increased the bandwidth, and improved significantly the instrument's sensitivity. In this paper, we present the first light of MEXART's digital system. We describe the new technical capabilities of the instrument, and we show some preliminary results: an estimation of the radio telescope's sensitivity ($\Delta S_{min} = 2.28 \pm 0.23$ Jy), the transit of the Galaxy at 140 MHz with the simultaneous tracking of 62 latitudinal beams, and an example of an IPS observation and the single-station methodology to calculate the solar wind speed. The new technical capabilities of the radio telescope will provide the potential to participate in several scientific studies. These include solar wind properties, space weather forecasting,

[4]Department of Astrophysics, University

of Oxford, UK

June 3, 2021, 6:55pm

ionospheric perturbations, and astrophysical aims such as monitoring of repeating Fast Radio Bursts (FRBs), and pulsars' observations.

1. Introduction

The Mexican Array Radio Telescope (MEXART) is a transit instrument mainly dedicated to performing Interplanetary Scintillation (IPS) observations with a central operating frequency of 139.65 MHz. The site is located in Coeneo, Michoacán, Mexico (19.81° N, 101.69° W) (Figure 1). The IPS phenomenon, detected by ground-based radio telescopes, is the random flux fluctuations of a radio source when its signal is scattered by the solar wind. These fluctuations are caused by the propagation of the solar wind's electron density irregularities causing a moving diffraction pattern along the line of sight (LOS). The recording of the radio source's transit shows flux intensity fluctuations (scintillation) with a periodicity around 1s. The scintillation level in the measurements is related to the variations of the solar wind electron density along the LOS. The IPS was discovered by Margaret E. Clarke during a 178 MHz interferometric survey of radio sources at Cambridge (Clarke, 1964). The phenomenon was analyzed and reported by Hewish, Scott, and Wills (1964).

An IPS technique to infer solar wind properties (speed and density fluctuations) is based on a power spectra analysis, where a Fast Fourier Transform is applied to the time series of the radio source transit. In general, there is a knee with a maximum around the 1 Hz regime, while the power decreases following a power law at higher frequencies. We fit the power spectrum to a physical model. This model

depends on several physical parameters (solar wind speed, the apparent source size, and the power index of the wavenumber of the density irregularities) (Scott et al., 1983; Manoharan & Ananthakrishnan, 1990; Mejia-Ambriz, 2012). This is known as the single-station methodology because it requires observations from only one radio telescope to calculate the solar wind speed.

To obtain reliable solar wind speed results with the single-station methodology, the observation of IPS should have a good signal-to-noise ratio, which depends on the radio telescope sensitivity. If the instrument cannot provide adequate IPS observations, the solar wind speed results of the fitting model would have, in general, larger errors (Chang et al., 2019).

MEXART's antenna is an array of 4096 full-wavelength dipoles ordered in a 64x64 element formation. The dipoles are arranged along 64 East-West (E-W) lines, covering a physical area of 8,401 m² (136.16 m (E-W) x 61.70 m (North-South N-S)). MEXART was originally operating with a 16x16 Butler matrix, which produced 16 fixed latitudinal beams (Gonzalez-Esparza et al., 2004). Using 1/4 of the antenna (16 E-W lines), MEXART undertook operations and reported the first measurements of IPS sources (Mejia-Ambriz et al., 2010), the detection of solar wind transient events (Romero-Hernandez et al., 2015), and the systematic observations of a few IPS sources to infer the yearly variation of their scintillation indexes (Chang et al., 2016). To improve the single-station fitting analysis, Aguilar-Rodriguez et al. (2014) presented a new technique based on the wavelet transform for analyzing MEXART IPS data.

MEXART's original system was based on analog technology. Figure 2 shows the block diagram of the signals, from the dipoles to the beam-former (Butler matrix). The signals detected by an E-W line of 64 dipoles are subdivided and collected in transmission lines into four sections of 16 dipoles each. The signal from each section passes through a high-pass filter, a first amplification step, and is combined 2:1 with the signal of the subsequent section. This resulting signal goes to a second combination level 2:1 at the middle of the line and a second amplification step, obtaining a final signal for the E-W line. The antenna with 64 E-W lines provides 64 inputs to the control room for beamforming and processing. The 16x16 Butler matrix was designed by engineers from the National Centre for Radio Astrophysics - Tata Institute of Fundamental Research in India, and it was assembled by the MEXART's team (Gonzalez-Esparza et al., 2004).

Although with MEXART's observations we were able to detect a few IPS sources to infer some solar wind's properties, the analog beamforming system presented several problems and limitations. The restriction of 16 input ports at the Butler matrix obligated us to further combine the antenna signals at the back-end to allow us to observe with half of the array (2:1 with 32 E-W lines) or the full array (4:1 with 64 E-W lines). This extra combination of the line signals produced larger errors in phase and amplitude that affected the beam formation. We tried several techniques to solve these issues, but our compensation solutions were only temporary. The 16 N-S beams produced by the Butler matrix had poor directivity (with very large secondary beams), which caused significant gain losses, and the instrument did not approach

the expected response. These technical problems prevented the radio telescope from detecting the number of radio sources required to monitor the solar wind between the Sun and the Earth. Furthermore, the IPS observations did not have a good signal-to-noise ratio for most of the radio sources, which is required by the single-station technique to obtain reliable solar wind parameters. We needed to upgrade the back-end system to reach the expected performance.

In 2014 the Mexican Space Weather Service was established to monitor and alert decision-makers about space weather conditions that compromise critical technologies in Mexico (Gonzalez-Esparza et al., 2017). Although space-based coronagraphs can detect the expulsion of coronal mass ejections in the solar atmosphere, their field of view is limited to a few dozen of solar radii. A very fast and geoeffective hypothetical coronal mass ejection, propagating towards the Earth's direction, could travel several hours without ground tracking until it reaches the L1 position, where a spacecraft would take in-situ measurements finally providing an early warning of only a few minutes. The IPS observations may be used as a remote sensing technique to measure solar wind disturbances, which can potentially detect solar wind's large-scale perturbations some hours (up to days) in advance before they reach 1 AU (Romero-Hernandez et al., 2015). The necessity of monitoring space weather conditions as well as to accomplish the aims of scientific studies, led us to improve the detection of IPS radio sources and, hence to upgrade MEXART's analog back-end to a digital system.

This paper presents the first light of MEXART's digital system. The outline of the paper is as follows: Section 2 describes the new technical capabilities of the digital instrument and compares them with the previous analog configuration. Section 3 shows some preliminary results: an estimation of the instrument's sensitivity, the observation of the transit of the Galaxy at 140 MHz, and an IPS observation where we used the single-station methodology to infer the solar wind speed. Section 4 comments on other possible scientific applications for the new radio telescope's capabilities, and Section 5 presents a summary.

2. MEXART digital upgrade: system specifications

Based on the necessity to improve the response of the radio telescope, we upgraded the back-end to a digital system. The description of the digital upgrade is described in detail elsewhere (Magro et al., 2019, 2021). Figure 3 shows a block diagram of the digital back-end. The signals of the 64 E-W lines travel through three levels of amplification, after which they are connected to the two FPGA boards. The beamformer system is generated by software running on a dedicated GPU server, which can generate different beam configurations (e.g., a synthetic beam pointing to any declination or 62 fixed latitudinal beams). The software can analyze the amplitude and phase of the 64 input digitalized signals. The system runs calibration observations to obtain correlation coefficients that compensate digitally (in phase and amplitude) the 64 signals from the antennas. By running a calibration observation on a routine basis, we corroborate the stability of the system. Figure 4 shows the

64 antenna signals arriving at the control room and connecting to the two FPGA boards. Table 1 summarizes some technical capabilities of the digital system and compares them with the analog configuration. The digital system, based on two FPGA boards and software, has new capabilities in beamforming, bandwidth, and frequency resolution. The digital system has a wider bandwidth of 12.5 MHz, covering a frequency range from 133.4 to 145.9 MHz, with a frequency resolution of 24.4 KHz (512 channels). Another advantage is that now the instrument has the capability of detecting with a higher sampling rate (1 ms). The digital system produced significant improvements in directivity and sensitivity, reaching the expected performance.

3. Preliminary results

3.1. Estimation of the array's sensitivity

The normalized one-dimensional beam pattern, P, (for a rectangular array of aperture l and observing wavelength λ) can be modeled as a function of the angular direction θ in the sky by

$$P(\theta) = \left(\frac{\sin(\Theta)}{\Theta} \right)^2 , \tag{1}$$

with $\Theta = \frac{\pi l}{\lambda} \sin(\theta)$. Figure 5 shows (red curve) MEXART's theoretical beam pattern along the E-W direction ($l_x = 136.16$ m, $\lambda = 2.14$ m). The pattern is proportional to the received signal power and to the output voltage $V = rP$, where r is the responsivity. The full width at half maximum (FWHM) of the beam is $0.89 \, \lambda/l_x$ radians or 0.80°, which corresponds to the width of the beam along the E-W direction. In a similar way, the beam along the N-S direction ($l_y = 61.7$) is 1.77°.

June 3, 2021, 6:55pm

Because of MEXART's geographic location (19.81° N), it is convenient to use 3C144 (SNR Crab Nebula) measurements to infer the antenna beam pattern and to estimate the instrument's sensitivity in full power. The radio flux of 3C144 is very well studied and has a flux density of 1395 Jy at 140 MHz (Perley & Butler, 2017). This radio source can be considered as a point source by MEXART's beams, and its transit is close to the local zenith. Figure 5 shows a transit of 3C144 observed by MEXART (black curve) compared with the expected beam pattern along the East to West direction (red curve). For this observation, we used the synthetic beam configuration to point the beam in full power mode towards the radio source. By analyzing 17 transits of 3C144 detected with the synthetic beam, we got a FWHM average of 0.86 ± 0.006 degrees. As is shown in Figure 5, the theoretical radiation pattern has a very good fitting to the observations, with the beam width having a relative error of 7%. The amplitude and direction of the side lobes also agree very well. As expected, the first side lobes are very close to 5% of the level of the main lobe.

With these observations we can estimate the instrument's sensitivity. The beam's solid angle through all the power Ω_A is related to the effective antenna aperture A_e as

$$A_e = \frac{\lambda^2}{\Omega_A}. \tag{2}$$

For a two dimensional array with beamwidths that are θ_x and θ_y, $\Omega_A = 1.3\,\theta_x\,\theta_y$ (Kraus, 1986). By assuming that the beam is about 7% wider along the N-S direction (1.89°), $A_e = 7115\,\mathrm{m}^2$. Therefore, an antenna efficiency of $\eta = 0.8$ can be assumed, with a gain of 42.9 dB in full power mode.

By analyzing 15 transits of 3C144 during February 2021 (using the full bandwidth $\Delta\nu = 12.5$ MHz and a sampling time $\tau = 20$ ms), the minimum detectable flux density is $\Delta S_{min} = 1395\,\mathrm{Jy}/\mathrm{N}_\sigma$, where N_σ is the observed intensity normalized to sigma noise ($\mathrm{N}_\sigma = I/\sigma_I$ units). From this, we get a minimum detectable flux $\Delta S_{min} = 2.28 \pm 0.23$ Jy.

Using ΔS_{min} we can estimate the temperature of the system T_s by

$$T_s = \frac{A_e\sqrt{\Delta\nu\,\tau}}{2\,K_B\,K_r}\Delta S_{min},\tag{3}$$

with $K_B =$ the Boltzmann constant and K_r is the sensitivity constant. In this case MEXART uses a correlation receiver characterized by $K_r = \sqrt{2}$ (Kraus, 1986). Table 2 shows the resulting ΔS_{min}, T_s and the sigma noise temperature of the system (ΔT) for three different bandwidths of the spectrometer.

The resulting $T_s = 1962$ K is higher than the value reported for the analog configuration with a shorter bandwidth ($T_s = 475$ K (Mejia-Ambriz et al., 2010)). This higher value in the system's temperature might be due to the filtering effect in the bandwidth added in the digital configuration, which attenuates the sensitivity at the two extremes of the bandwidth. MEXART's digital system has a sensitivity's peak around $\sim 135 - 142$ MHz, and the rest of the bandwidth tend to have a lower sensitivities.

For an ideal case (having maximum sensitivity across the entire bandwidth), we can use the best 24.4 KHz channel to calculate Ts. For an observation of 3C144, using the above analysis, a central channel detects the transit of the source with $\Delta S_{min} = 23$ Jy. By using Equation 3 in this case $T_s = 787$ Jy. For this ideal

case, with all channels responding with the same sensitivity, ΔS_{min} would be < 1 Jy. Subtracting the value of 295 K of the sky temperature at 140MHz (McKinley et al., 2012), the temperature of the instrument would be 492 K.

3.2. Mapping observations of 140 MHz radio sky

One of the limitations of the former analog system was the poor directivity of the 16 latitudinal beams produced by the Butler matrix. The N-S beam pattern had secondary beams with significant high gains, and the power of the secondary beams was comparable with the main beams. This directivity issue prevented the possibility of mapping the radio sky with the 16 latitudinal beams. As commented on before, the digital system allows different configurations of latitudinal beams. Figure 6 shows MEXART's digital configuration of 62 fixed latitudinal beams. The 62 beams point at different well-defined declinations. Using this configuration, along with the Earth's rotation, it is possible to measure the flux of the transit of the Galaxy. Figure 7 shows an observation of the transit of the Galaxy at 139.65 MHz detected by MEXART on April 10th, 2021. We used an integration time of 1.5 s for this observation. The plot shows the integrated flux density (512 frequency channels) as detected by the 62 latitudinal beams versus sidereal time. Each beam tracks a latitudinal band across the radio sky. The comparison of the 62 records shows the transit of the Galaxy at different declinations. The shapes of the Galaxy's nucleus and arm appear clearly in the combined curves. The Sun is the strongest radio source in the sky, which transited at 1:20 ST, 3C405 (Cygnus A) at 19:59 ST, 3C461 (Cassiopeia A) at 23:23 ST, and 3C144 (Crab Nebula) at 5:34 ST.

Figure 8 shows the contours of the transit of the Galaxy at 139.65 MHz using the measurements of the 62 fixed declination beams. This is the same observation as Figure 7, but in this case we removed the interferences and applied a numerical filter to smooth the gradients. We overplot contour curves to emphasize the radio flux zones in the Galaxy. The plot shows the transit of the strong sources commented on in Figure 7. This observation clearly shows that the 62 latitudinal beams' configuration have good directivity and now the radio telescope is able to track the radio sky.

3.3. IPS observations

The main aim of MEXART's upgrade is to improve the response in observing IPS sources. Figure 9 shows an example of an observation of the radio source 3C48 (J0137 + 331) on April 8, 2021. Figure 9(a) shows the record of the observation, at normalized intensity, which begins at 19:11:06 UT and ends at 19:25:53 UT. The temporal resolution of the data is 20 ms (50 records/s). We analyze the observation to obtain a power spectrum that highlights the IPS characteristics and eliminates, as far as possible, the contributions from various noise sources (satellite signals, electric storms, and local electromagnetic emissions). First, we remove any potential low-frequency trend from the time series to eliminate possible contributions by ionospheric scintillation. Therefore, we subtracted the running mean of 10 s, which equals 500 data in the time series. Figure 9(a) shows the IPS characteristic signature during the transit of 3C48. After the transit, it is also possible to observe contamination in the time series because of noise sources. Figure 9(b) shows the application of the wavelet transform (WT) to the time series (already treated) using the code of

Torrence and Compo (1998). Previous studies of MEXART's observations have used the WT for the analysis of IPS observations; see Aguilar-Rodriguez et al. (2014, 2015) and Romero-Hernandez et al. (2015). The square formed by the dotted line indicates the region in which the IPS is present. In terms of frequency, the square covers the range from 0.3 Hz to 2 Hz. It is possible to calculate the average spectral power within the square, which is equivalent to calculating the scintillation index (Aguilar-Rodriguez et al., 2014) and is given by $m = \sqrt{\langle P_{wt} \rangle - \langle P_{wt-sn} \rangle}$, where $\langle P_{wt} \rangle$ is the average spectral power inside the square and $\langle P_{wt-sn} \rangle$ is the average spectral power of the system noise at high frequencies, which we consider in the range from ~ 2 to ~ 10 Hz. Moreover, from the WT we can obtain the power spectrum of the signal. This is accomplished by averaging each frequency channel of the WT of the signal, which translates into an average spectral power value for each frequency. With this, a spectral power-frequency pair arrangement is formed. Figure 9(c) shows the power spectrum obtained from the spectral power-frequency pairs.

Once the observed power spectrum of the 3C48 radio source has been obtained, we perform the speed calculation using the single-station analysis methodology (Manoharan & Ananthakrishnan, 1990). We followed the methodology used in a previous analysis (Mejia-Ambriz et al., 2015; Chang et al., 2016, 2019). Figure 10 shows the fit of the theoretical spectrum with the observed one. The solar wind speed turns out to be 746 km/s, which corresponds to a fast solar wind stream. Figure 9(d) shows a schematic of the apparent location in the sky of the radio source 3C48 (red dot) at the moment of the observation, which was at ~ 26.4 degrees of elongation.

The center of Figure 9(d), shows an image of the Sun observed on April 8, 2021 by the Atmospheric Imaging Assembly (AIA) onboard the Solar Dynamics Observatory (SDO) mission. It can be seen that the radio source emission was above the solar disk, in which a polar coronal hole can be seen. The fast solar wind obtained from the IPS analysis agrees with the LOS of the source crossing the radial direction to the polar coronal hole.

4.   Other applications besides IPS observations

The main scientific objective of the instrument is to perform daily observations of IPS sources (during the daytime). The good sensitivity and directivity of the radio telescope would allow performing routinely measurements of at least a few dozen of IPS sources to provide solar wind data that can be used for space weather forecasting purposes. MEXART's observations would complement the daily IPS measurements by the ISEE antennas of the Nagoya University (Tokumaru et al., 2011), which had provided daily solar wind data for several years. The new technical capabilities from the digital upgrade allow us also to plan further observations. We present a shortlist of possible applications for other astrophysical studies. (1) Monitoring of repeating Fast Radio Bursts (FRBs), periods of 10-100s of days requires a great deal of telescope time and MEXART is capable of forming multiple beams to monitor several repeaters. (2) Surveying for new FRBs. (3) Observations of pulsars, we can reduce the sampling time to 5.2 μs , which is typical for pulsar observations and we

have a good number of frequency sub bandwidths. (4) Measurements of ionospheric scintillation. (5) Solar radio bursts, and (6) observations of Jupiter flares.

5. Summary

The first results presented in this paper show that the directivity problems of MEXART's beamforming analog system were solved completely with the new digital back-end. The radio telescope now has new technical capabilities that significantly improve its performance: higher sensitivity, wider bandwidth, and 512 frequency channels. The digital system can measure the gain and the phase of the 64 input signals coming from the antenna, and by using calibration coefficients in can compensate for the signal differences. We presented the first observations to show that two different beam configurations (a synthetic beam and 62 fixed latitudinal beams) obtained good observations with the expected beam patterns and sensitivity. Future work includes the elaboration of a new catalog of IPS sources, software to clean the frequency bands of interferences, the participation in international campaigns of solar wind studies, the automation of the IPS single-station methodology to produce solar wind data for space weather forecasting, and the extension of the instrument's observations for other astrophysical studies.
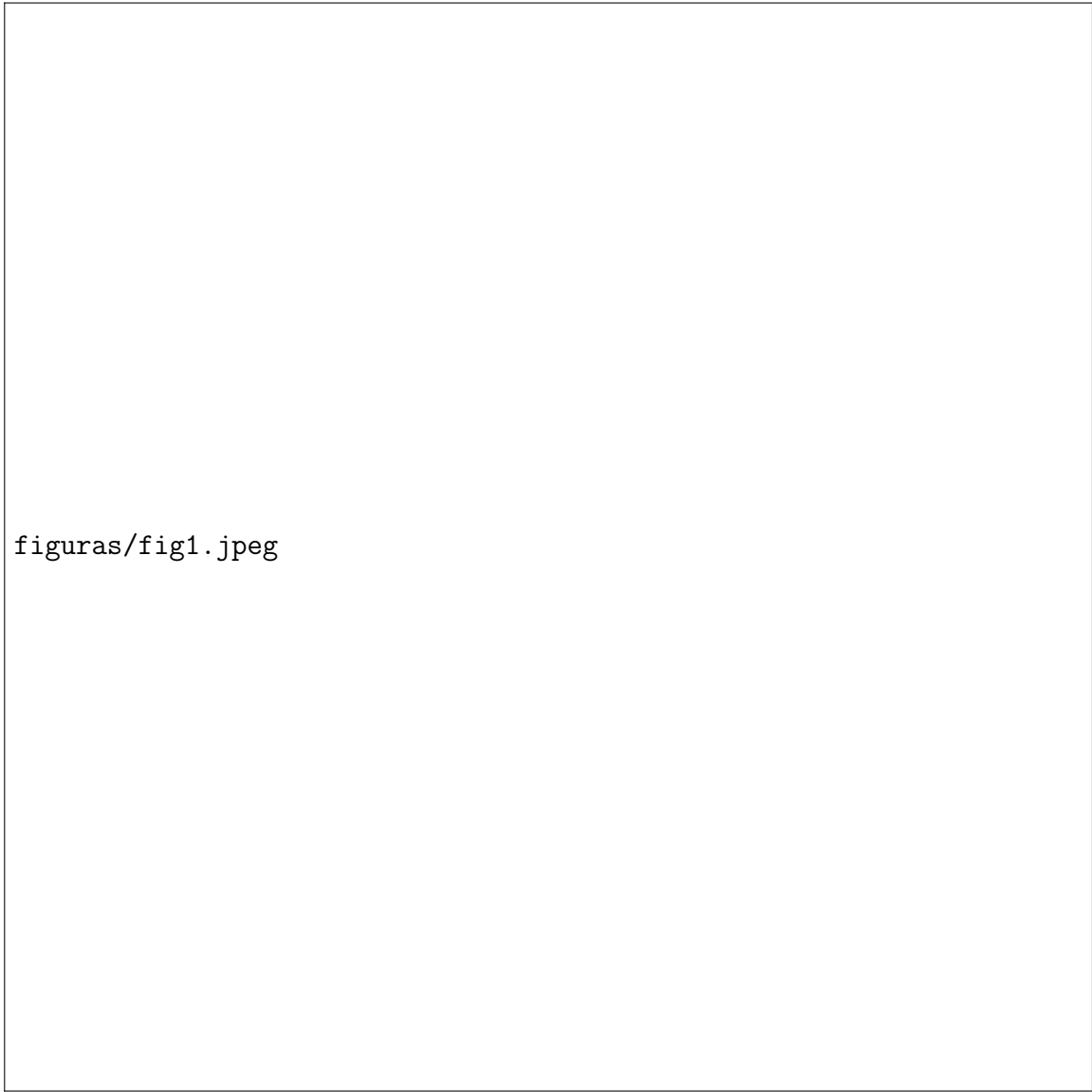
June 3, 2021, 6:55pm

References

Aguilar-Rodriguez, E., Mejia-Ambriz, J. C., Jackson, B. V., Buffington, A., Romero-Hernandez, E., Gonzalez-Esparza, J. A., . . . Manoharan, P. K. (2015). Comparison of solar wind speeds using wavelet transform and fourier analysis in ips data. *Solar Physics*, *290*, 2507-2518. doi: 10.1007/s11207-015-0758-0

Aguilar-Rodriguez, E., Rodriguez-Martinez, M., Romero-Hernandez, E., Mejia-Ambriz, J. C., Gonzalez-Esparza, J. A., & Tokumaru, M. (2014). The wavelet transform function to analyze interplanetary scintillation observations. *Geophys. Res. Lett.*, *41*, 3331-3335. doi: 10.1002/2014GL060047

Chang, O., Bisi, M., Aguilar-Rodriguez, E., Fallows, R. A., Gonzalez-Esparza, J. A., Chashei, I., & Tyul'bashev, S. A. (2019). Single-site ips power spectra analysis for space weather products using cross-correlation function results from eiscat and merlin ips data. *Space Weather*, *17*, 1114-1130. doi: 10.1029/2018SW002142

Chang, O., Gonzalez-Esparza, J. A., & Mejia-Ambriz, J. C. (2016). Ips observations at 140 mhz to study solar wind speeds and density fluctuations by mexart. *Advances in Space Research*, *57*, 1307-1313.

Clarke, M. E. (1964). *Two topics in radiophysics. i. some observations of discrete radio sources. ii. an investigation of ionospheric irregularities using a radio signal from an artificial satellite* (5097). University of Cambridge.

Gonzalez-Esparza, J. A., Aguilar-Rodriguez, E., Mejia-Ambriz, J. C., Villanueva-Hernández, P., & Andrade-Mascote, E. (2021, June). *First observations of the new mexart's digital system (version 1.0) [data set]. zenodo.* doi: 10.5281/zenodo.4891337

Gonzalez-Esparza, J. A., Carrillo, A., Andrade, E., R., P., & Kurtz, S. (2004). The mexart interplanetary scintillation array in mexico. *Geofisica Internaciona*, *43*(1), 61-73.

Gonzalez-Esparza, J. A., De la Luz, V., Corona-Romero, P., Mejia-Ambriz, J. C., Gonzalez, L. X., Sergeeva, M. A., . . . Aguilar-Rodriguez, E. (2017). Mexican space weather service (sciesmex). *Space Weather*, *15*(1), 3-11. Retrieved from `https://agupubs.onlinelibrary.wiley.com/doi/abs/10.1002/2016SW001496` doi: https://doi.org/10.1002/2016SW001496

Hewish, A., Scott, P., & Wills, D. (1964). Interplanetary scintillation of small diameter radio sources. *Nature*, *203*.

Kraus, J. D. (1986). *Radio astronomy* (2nd edition ed.). McGraw-Hill.

Magro, A., Chiello, R., Cutajar, D., Borg, J., Zarb-Adami, K., Gonzalez-Esparza,

J. A., ... Andrade-Mascote, E. (2019). A new digital backend for the mexican array radio telescope. In *2019 international conference on electromagnetics in advanced applications (iceaa)*. doi: 10.1109/ICEAA.2019.8878959

Magro, A., Chiello, R., Cutajar, D., Borg, J., Zarb-Adami, K., González-Esparza, J. A., ... Andrade-Mascote, E. (2021).
in preparation.

Manoharan, P., & Ananthakrishnan, S. (1990). Determination of solar-wind velocities using single-station measurements of interplanetary scintillation. *Mon. Not. Roy. Astron. Soc.*, *244*, 691.

McKinley, B., Briggs, F., Kaplan, D. L., Greenhill, L. J., Bernardi, G., Bowman, J. D., ... Wyithe, J. S. B. (2012, dec). LOW-FREQUENCY OBSERVATIONS OF THE MOON WITH THE MURCHISON WIDEFIELD ARRAY. *The Astronomical Journal*, *145*(1), 23. Retrieved from `https://doi.org/10.1088%2F0004-6256%2F145%2F1%2F23` doi: 10.1088/0004-6256/145/1/23

Mejia-Ambriz, J. C. (2012). *Análisis de observaciones del mexart: bases para estudios de centelleo interplanetario* (Unpublished doctoral dissertation). Posgrado en Ciencias de la Tierra, Universidad Nacional Autónoma de México.

Mejia-Ambriz, J. C., Jackson, B. J., González-Esparza, J. A., Buffington, A., Tokumaru, M., & Aguilar-Rodriguez, E. (2015). Remote-sensing of solarwind speeds from ips observations at 140 and 327 mhz using mexart and stel. *Solar Physics*, 2539-2552. doi: 10.1007/s11207-015-0694-z
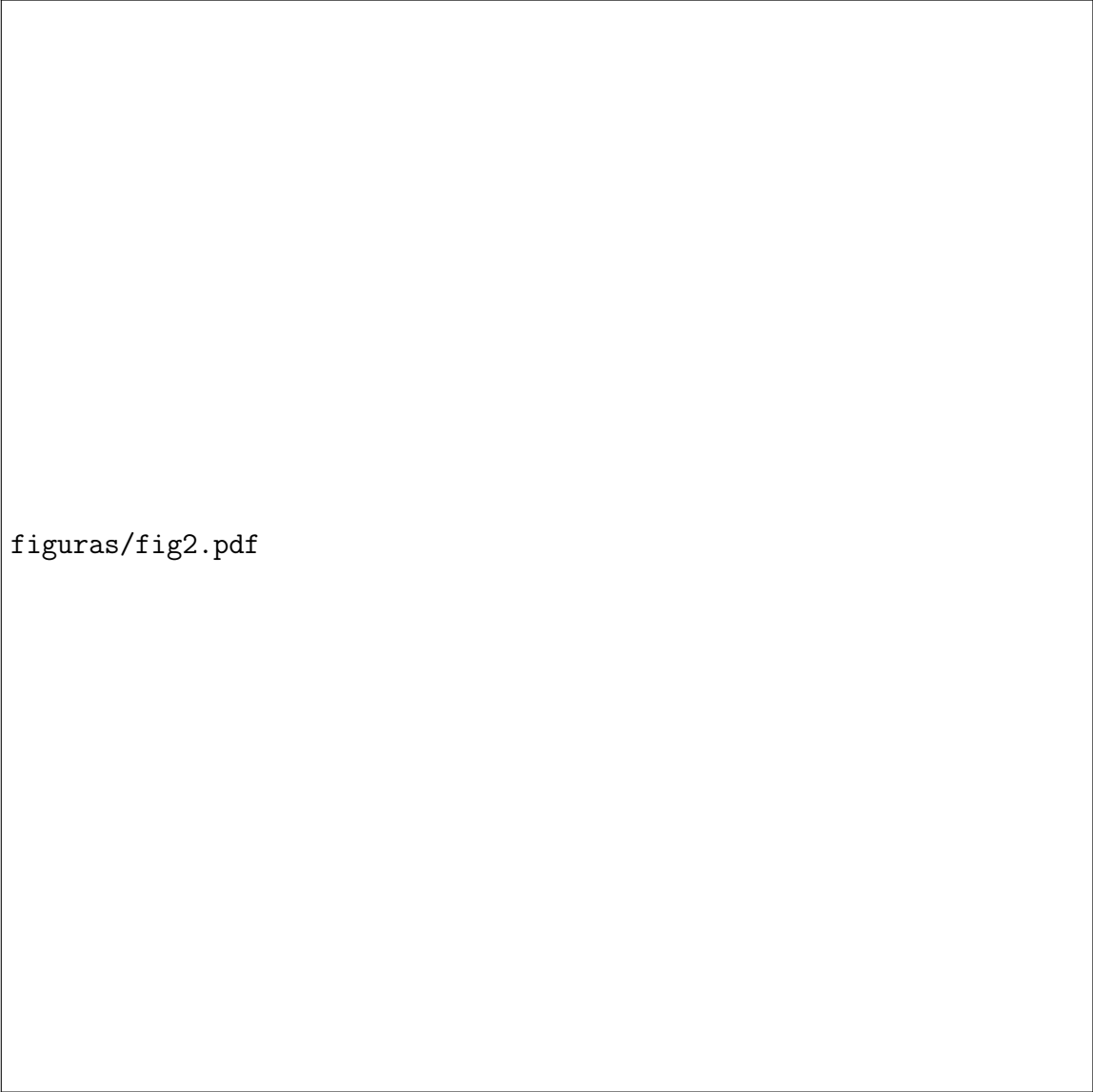
Mejia-Ambriz, J. C., Villanueva-Hernandez, P., González-Esparza, J. A., Aguilar-Rodriguez, E., & Jeyakumar, S. (2010). Observations of interplanetary scintillation (ips) using the mexican array radio telescope (mexart). *Solar Physics*, *265*(1), 309-320,. doi: 10.1007/s11207-010-9562-z

Perley, R. A., & Butler, B. J. (2017). An accurate flux density scale from 50 MHz to 50 GHz. *The Astrophysical Journal Supplement Series*, *230*(1), 7. Retrieved from `https://doi.org/10.3847%2F1538-4365%2Faa6df9` doi: 10.3847/1538-4365/aa6df9

Romero-Hernandez, E., Gonzalez-Esparza, J. A., Aguilar-Rodriguez, E., Ontiveros-Hernandez, V., & Villanueva-Hernandez, P. (2015, may). Detection of solar wind disturbances: Mexican array radio telescope IPS observations at 140 MHz. *Solar Physics*, *290*(9), 2553–2566. Retrieved from `https://doi.org/10.1007%2Fs11207-015-0690-3` doi: 10.1007/s11207-015-0690-3

Scott, S., Coles, W. A., & Bourgois, G. (1983). Solar wind observations near the sun using interplanetary scintillation. *Astron. Astrophys*, *123*(207).

Tokumaru, M., Kojima, M., Fujiki, K., Maruyama, K., Maruyama, Y., Ito, H., & Iju, T. (2011). A newly developed uhf radiotelescope for interplanetary scintillation observations: Solar wind imaging facility. *Radio Science*, *46*(5). Retrieved from `https://agupubs.onlinelibrary.wiley.com/doi/abs/10.1029/2011RS004694` doi: https://doi.org/10.1029/2011RS004694

Torrence, C., & Compo, G. P. (1998). A practical guide to wavelet analysis. *Bulletin of the American Meteorological Society*, *79*(1), 61-78. doi: 10.1175/1520-0477
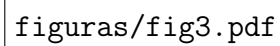
```
figuras/fig1.jpeg
```

Figure S1. Panoramic view of the MEXART site (19.81° N, 101.69° W).

figuras/fig2.pdf

Figure S2. Block diagram of the MEXART's antenna signals processes and its original beam forming analog system (16x16 Butler matrix).
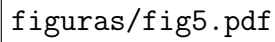
figuras/fig3.pdf

Figure S3. Block diagram of the new MEXART's digital back-end.

figuras/fig4a.png

figuras/fig4b.png

figuras/fig4d.png

figuras/fig4c.png

Figure S4. Pictures of the MEXART's digital back-end at the control room.

Table S1. Comparison of the characteristics of the two MEXART's configurations: analog and digital systems.

parameter	analog system	digital system
beam former	Butler matrix	FPGA firmware and software
central frequency	139.65 MHz	139.65 MHz
banwidth	1.5 MHz	12.5 MHz
frequency channels	1	512
latitudinal beams	16	several configurations
sensitivity	1/4 array → 20-30 Jy	full array → 2.3 Jy
	1/2 array → 15 Jy	
	full array → 20 Jy	
sampling rate	20 ms	40.96 bus, integration time (0.5ms-2s)
extra capabilities		real time monitoring of the input antenna signals
		amplitude and phase corrections
		observation management
		web-based dashboard

June 3, 2021, 6:55pm
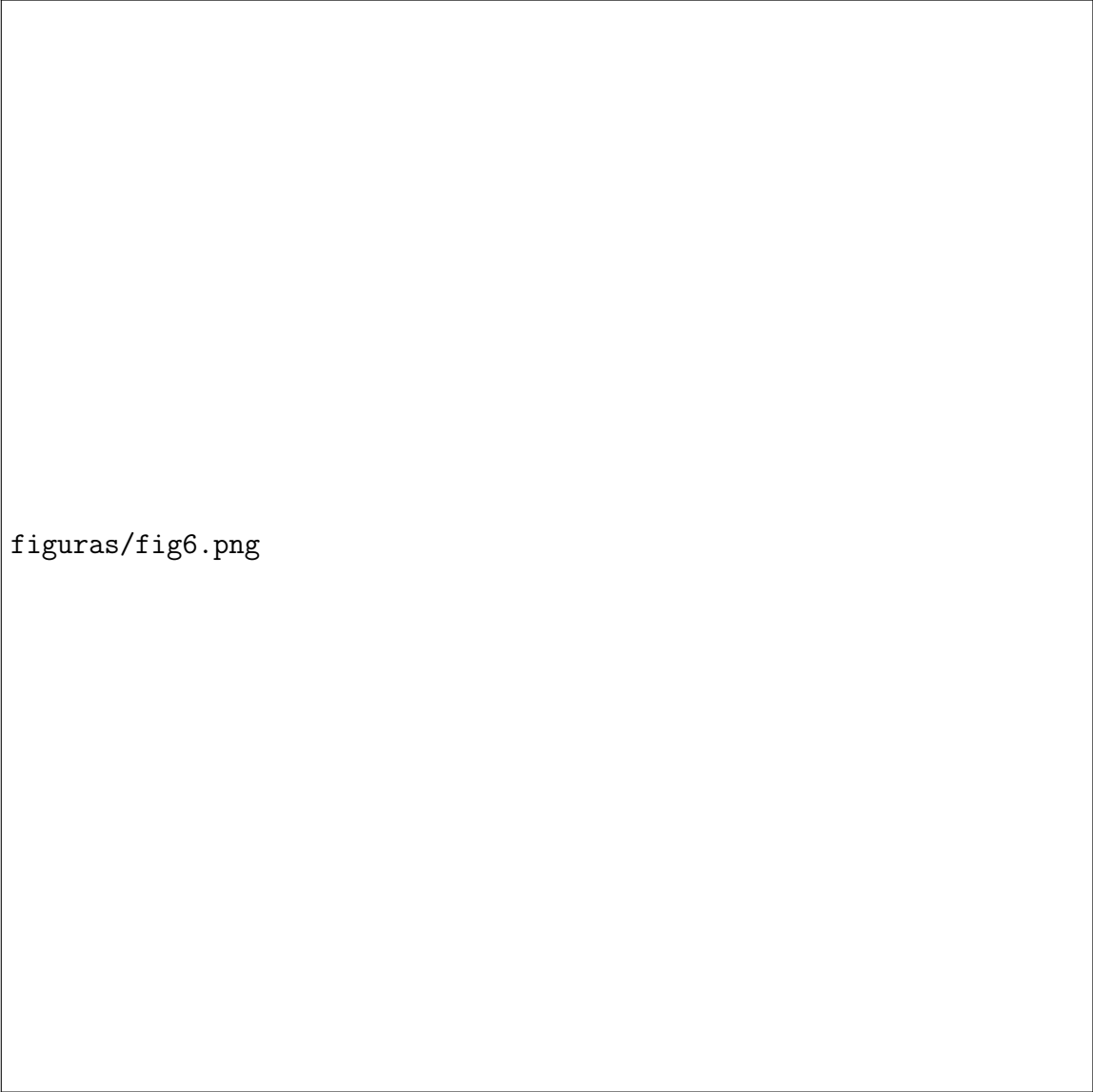
figuras/fig5.pdf

Figure S5. Digital system. Comparison (overlapping plots) between the theoretical beam pattern (red curve) and the measurement of the transit of a calibration source (3C144) (black curve). The two curves show an excellent agreement. The MEXART's E-W beam pattern in full power performs as expected.

Table S2. Estimation of the minimum flux detected by MEXART's digital back-

end and the system temperature for different bandwidths.

$\Delta\nu$	ΔS_{min} (Jy)	T_s (K)	ΔT (K)
24.4 KHz	23.45	891	57.0
2 MHz	3.55	1222	8.6
12.5 MHz	2.28	1962	5.5

figuras/fig6.png

Figure S6. Digital system. Configuration of 62 fixed latitudinal beams at different declinations. Normalized electric far-field amplitude. The total angular coverage in the meridian is $\pm 72.4°$ respecto to the zenith. The beam pattern follows $\pm \sin(\delta) = (n - 1/2)/32$, where n is the beam number (from 1 to 31) and δ is the angle between the local zenith and the beam direction.
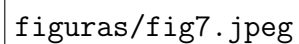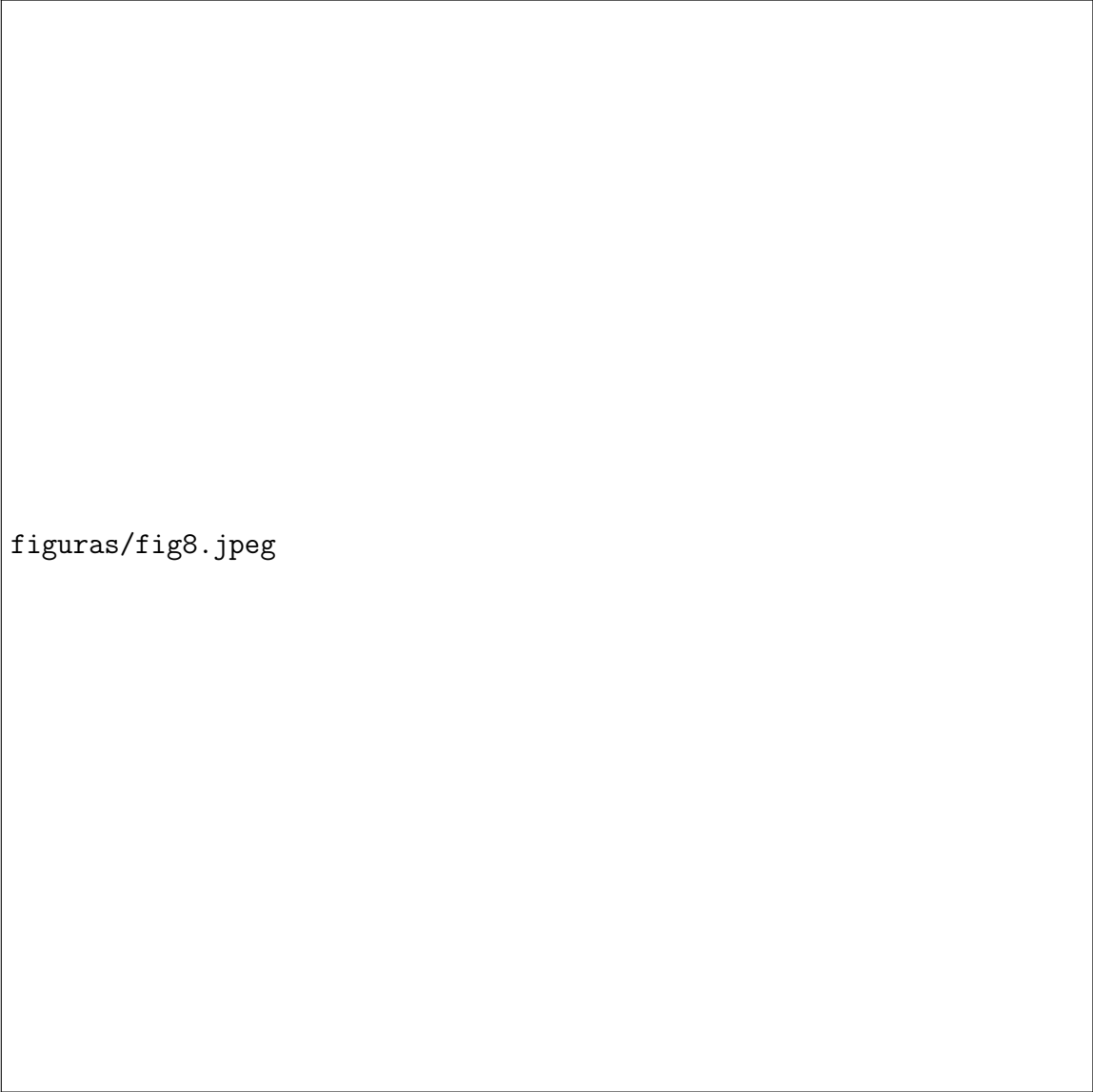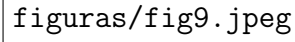
figuras/fig7.jpeg

Figure S7. Integrated flux measurements of the 62 latitudinal beams indicating the transit of the Galaxy on 2021-04-10. Horizontal axis: sideral time, vertical axis: integrated flux detected by the latitudinal beams at different declinations.
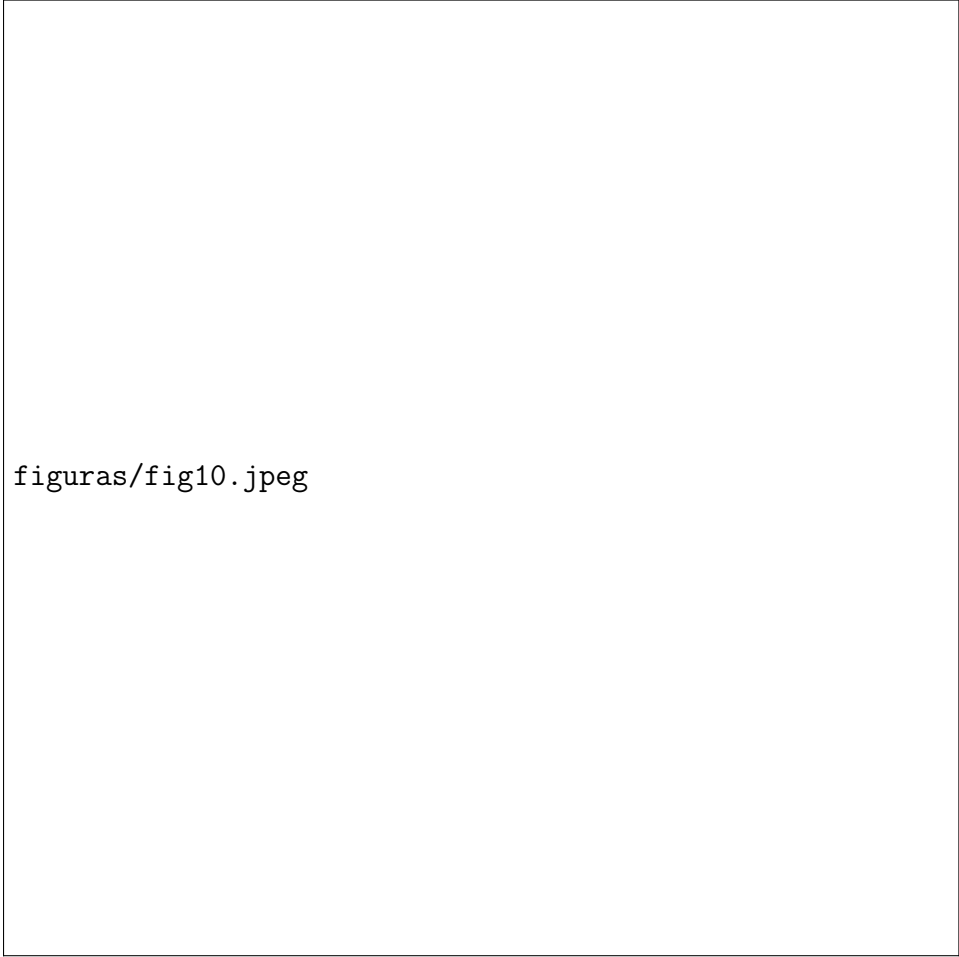
figuras/fig8.jpeg

Figure S8.   Transit of the Galaxy detected by MEXART at 140 MHz on 2021-04-10. Horizontal axis: sideral time, vertical axis: latitudinal beams, color contours: radiation flux. Observation with 62 fixed latitudinal beams at different declinations.

Figure S9. Measurement of the transit of an IPS radio source detected by MEXART and data analysis to infer solar wind values. (a) Time series of the radio source 3C48 observed by MEXART on 2021-04-10. (b) WT applied to the time series, which allows us to identify regions where IPS is present. The dashed lines indicate the frequency range where IPS is commonly observed (i.e., from 0.3 Hz up to 2 Hz). (c) Power spectra of 3C48 at 140 MHz. (d) Relative position of 3C48 (red point) with respect to the Sun. The Earth's direction is perpendicular to the plane. The line of sight of the radio source was crossing the region covered by a fast solar wind stream from the northern coronal hole.

figuras/fig10.jpeg

Figure S10. Single-station solar wind speed analysis for the observation of 3C48 on 2021-04-10 . The single-station model fitting obtains a solar wind speed of 746 km/s.
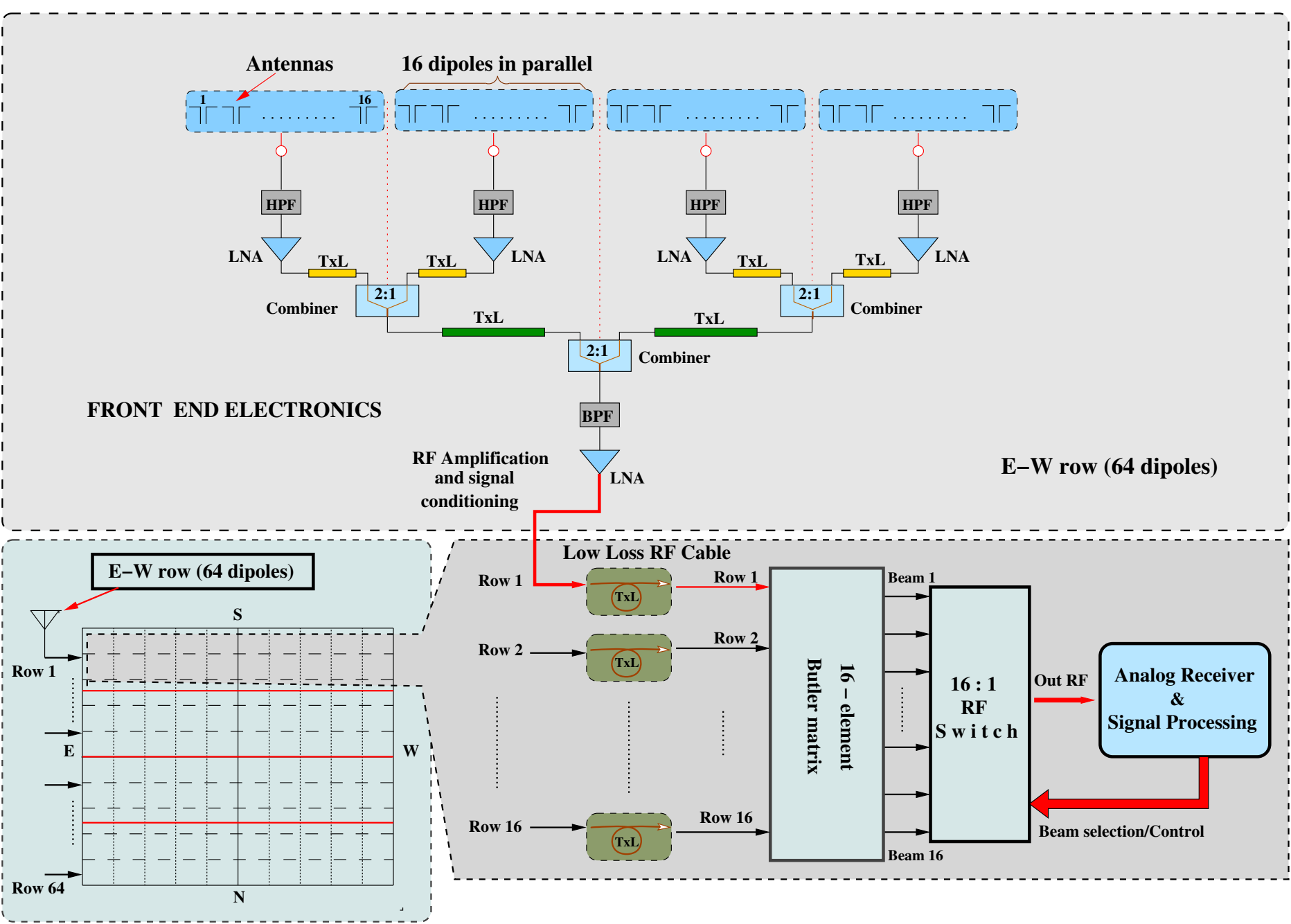
Figure 1.

Figure 2.
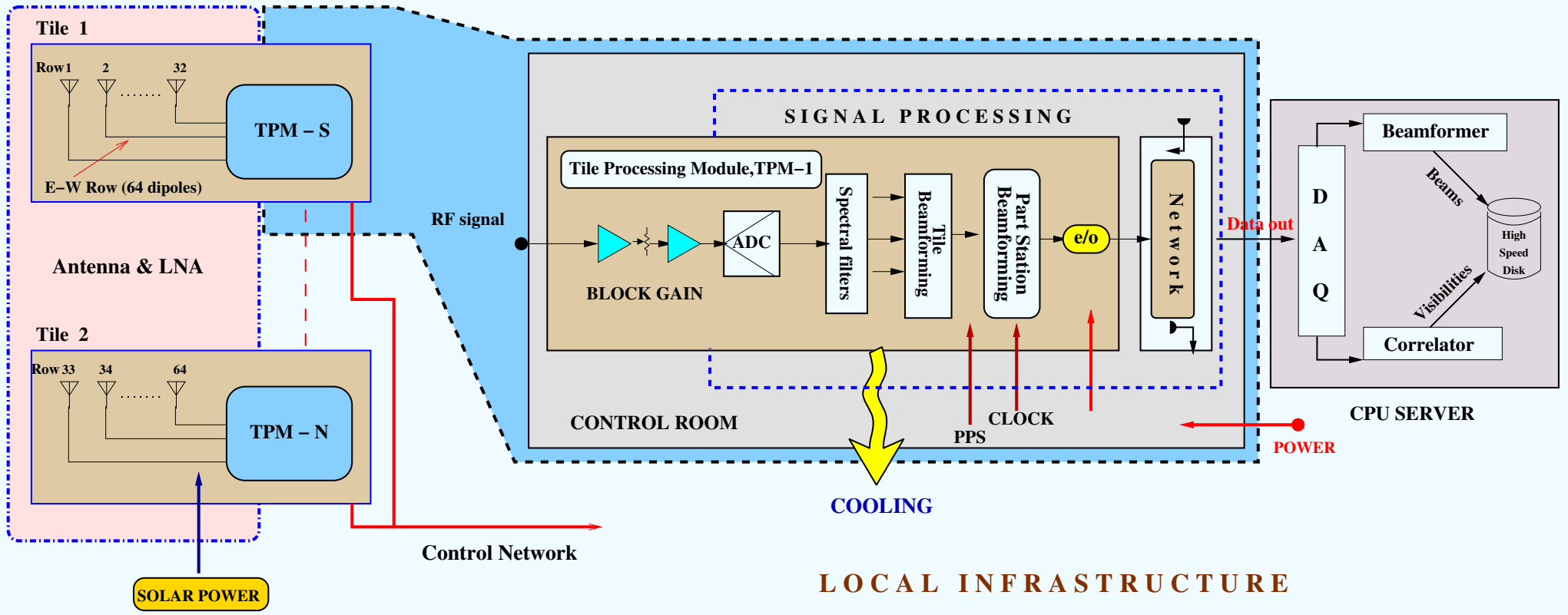
Antennas

16 dipoles in parallel

1 16

HPF HPF HPF HPF

LNA TxL TxL LNA LNA TxL TxL LNA

Combiner **2:1** **2:1** Combiner

TxL TxL

2:1 Combiner

BPF

FRONT END ELECTRONICS

E−W row (64 dipoles)

RF Amplification
and signal
conditioning

LNA

E−W row (64 dipoles)

S

Row 1

E W

Row 64

N

Low Loss RF Cable

Row 1 TxL Row 1 Beam 1

Row 2 TxL Row 2

Row 16 TxL Row 16

**16 – element
Butler matrix**

Beam 16

**16 : 1
RF
Switch**

Out RF

**Analog Receiver
&
Signal Processing**

Beam selection/Control

Figure 3.

Figure 4a.

Figure 4b.

Figure 4c.

Figure 4d.
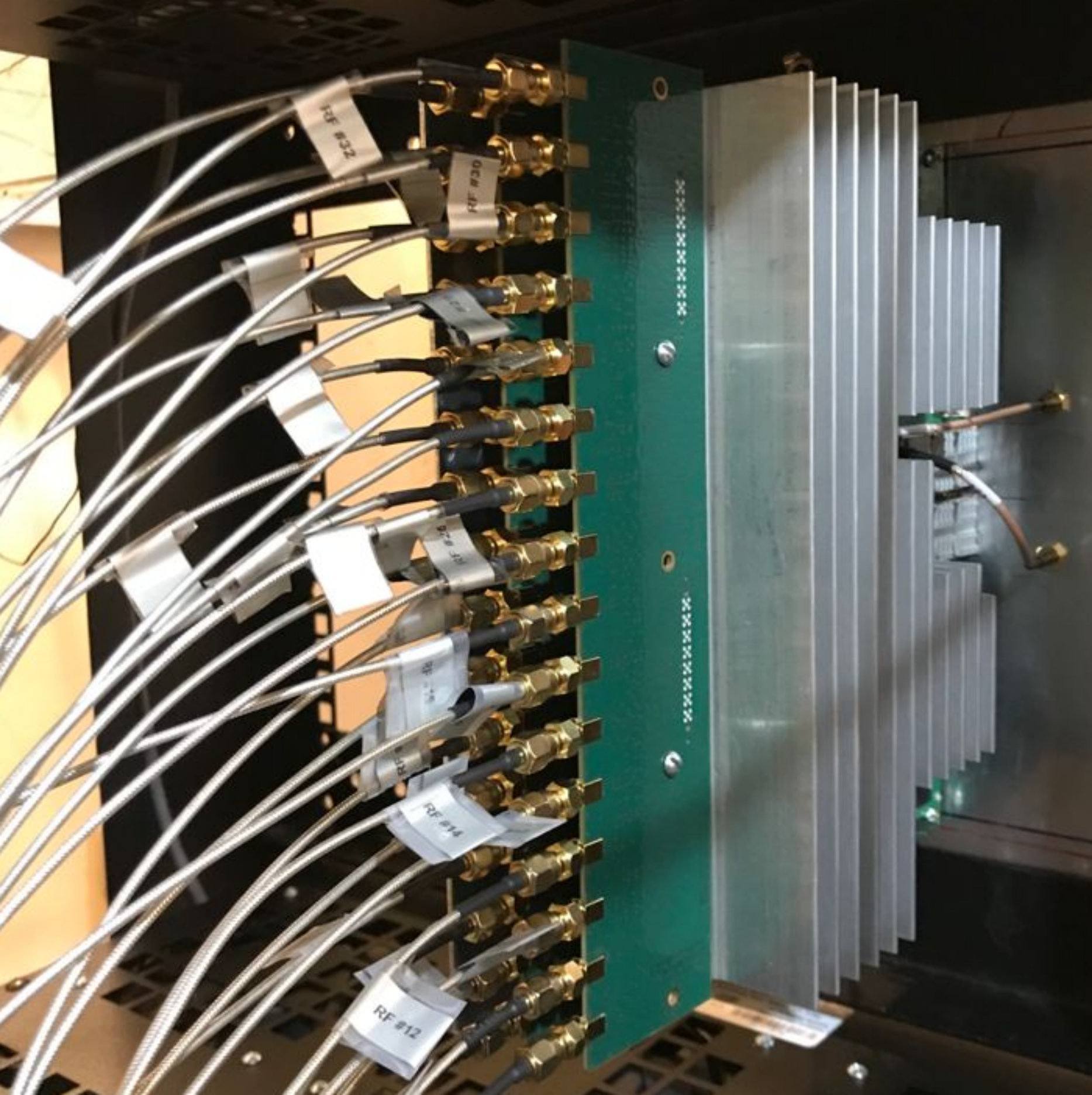
Figure 5.

Modeling of radiation pattern and Crab Nebula transit

Obs FWHM = 0.85

Expected FWHM = 0.80

Modeling

Transit 20210202

Normalized power

θ (degrees)

Figure 6.

S   N

1   1

0.5   0.5

1   0.5   0   0.5   1
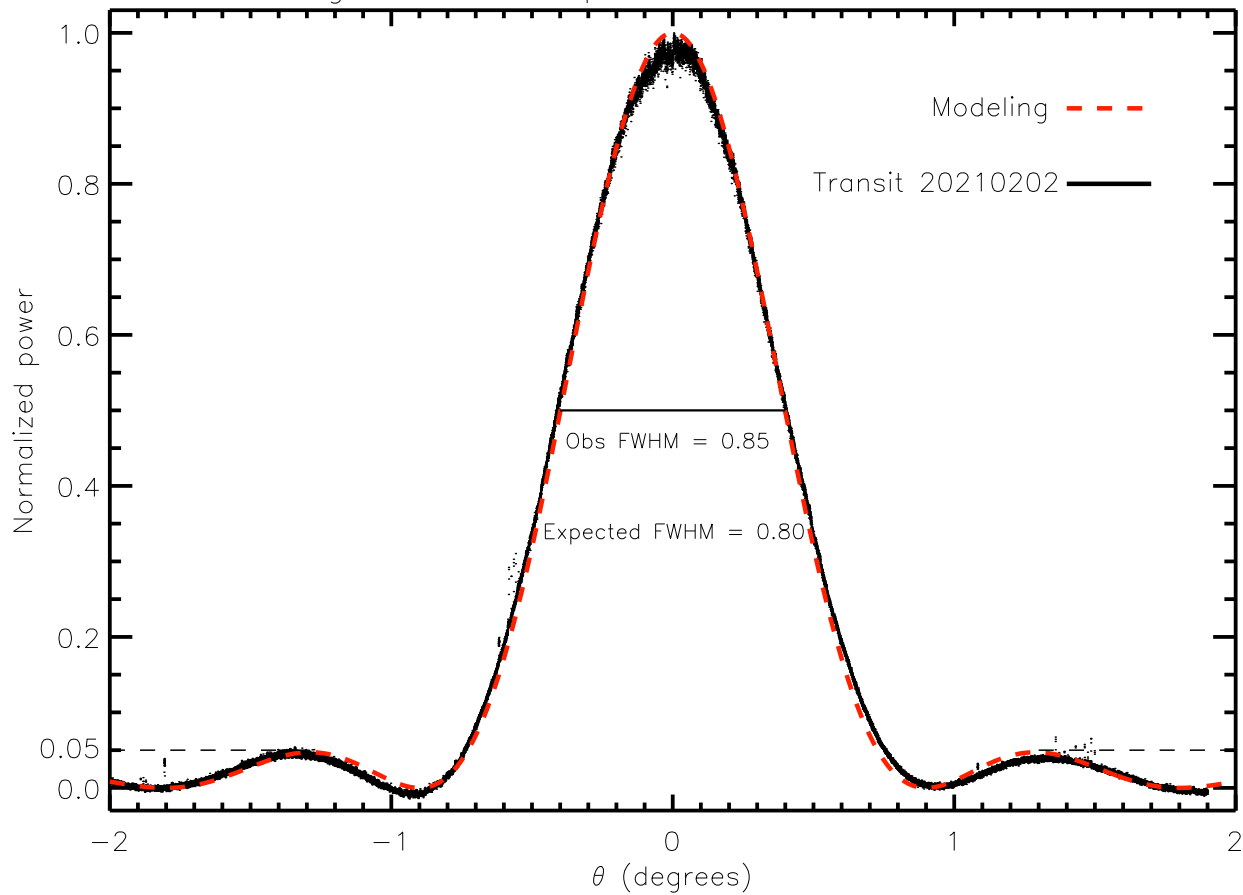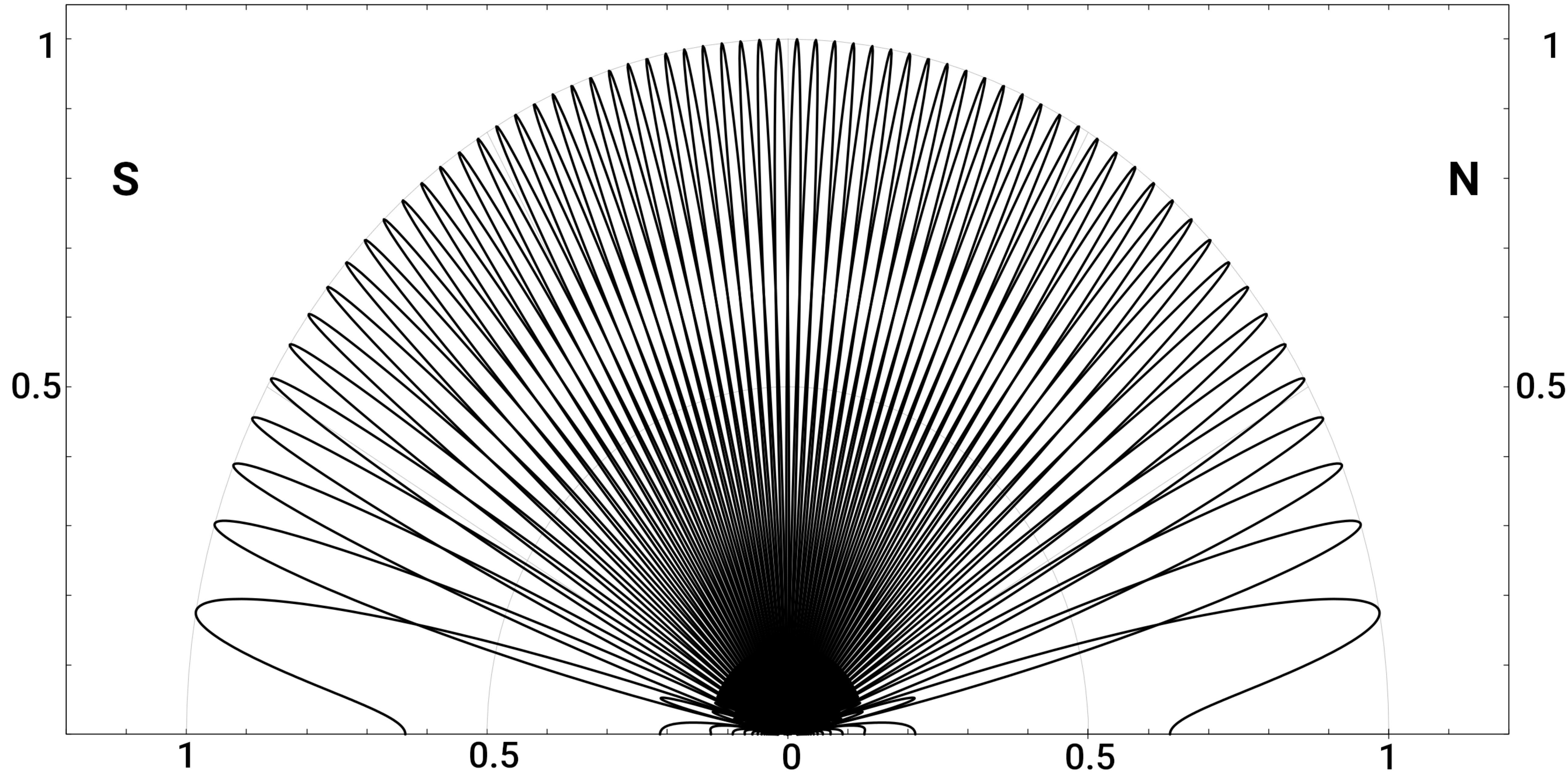
Figure 7.

MEXART Beams @ 140 MHz (April 10, 2021)
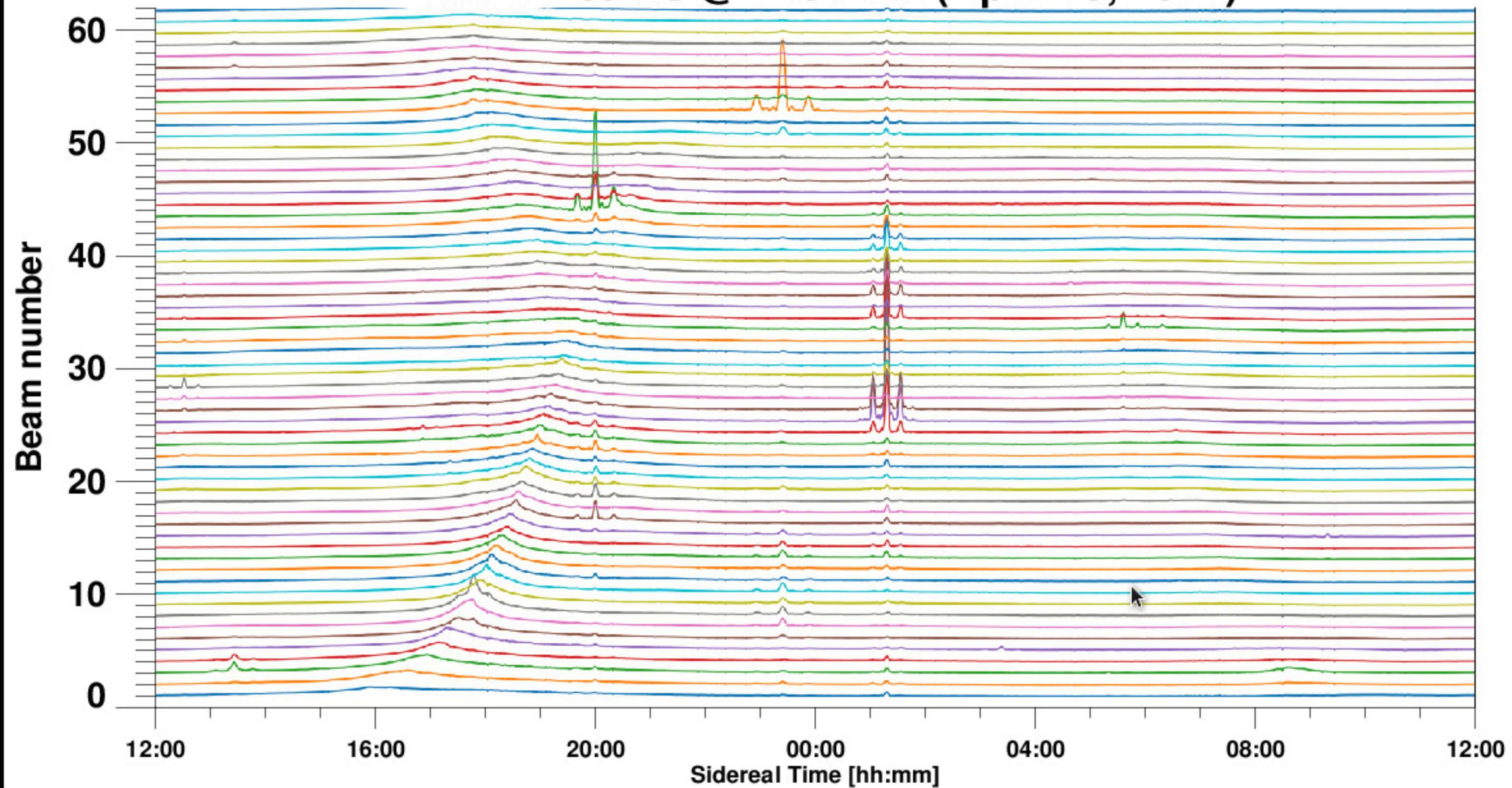
Figure 8.

MEXART Radio Sky @ 140 MHz (April 10, 2021)
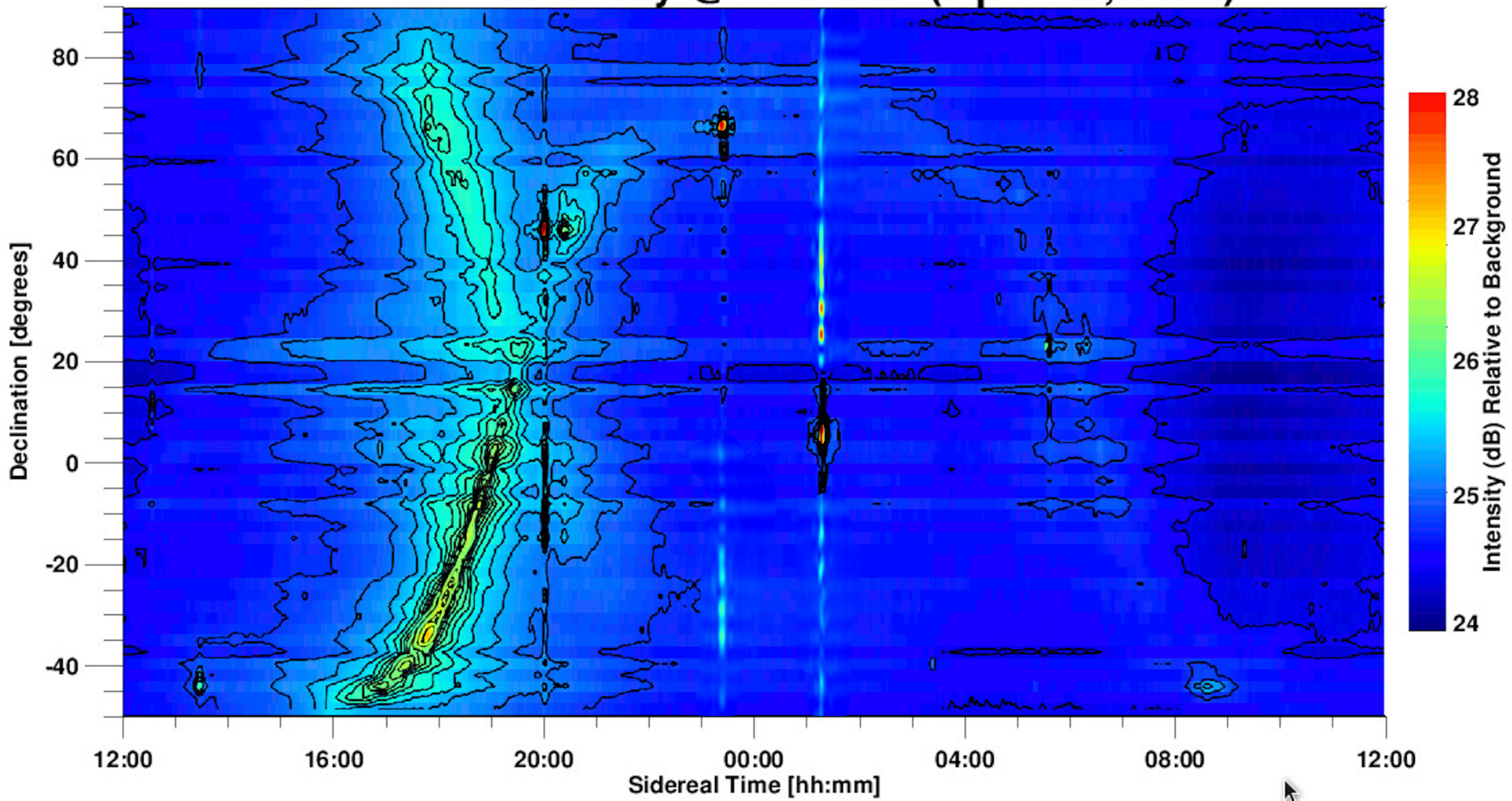
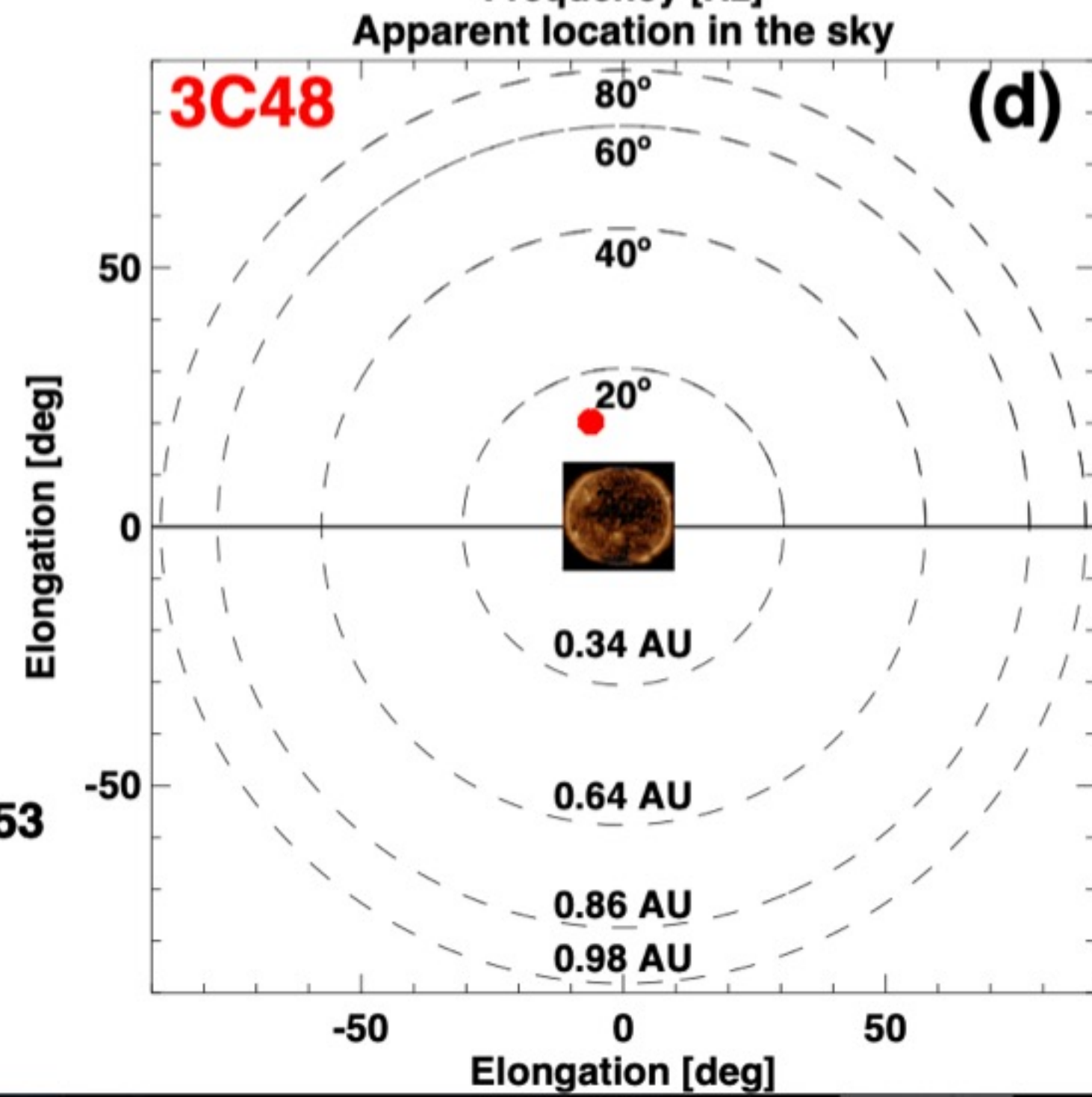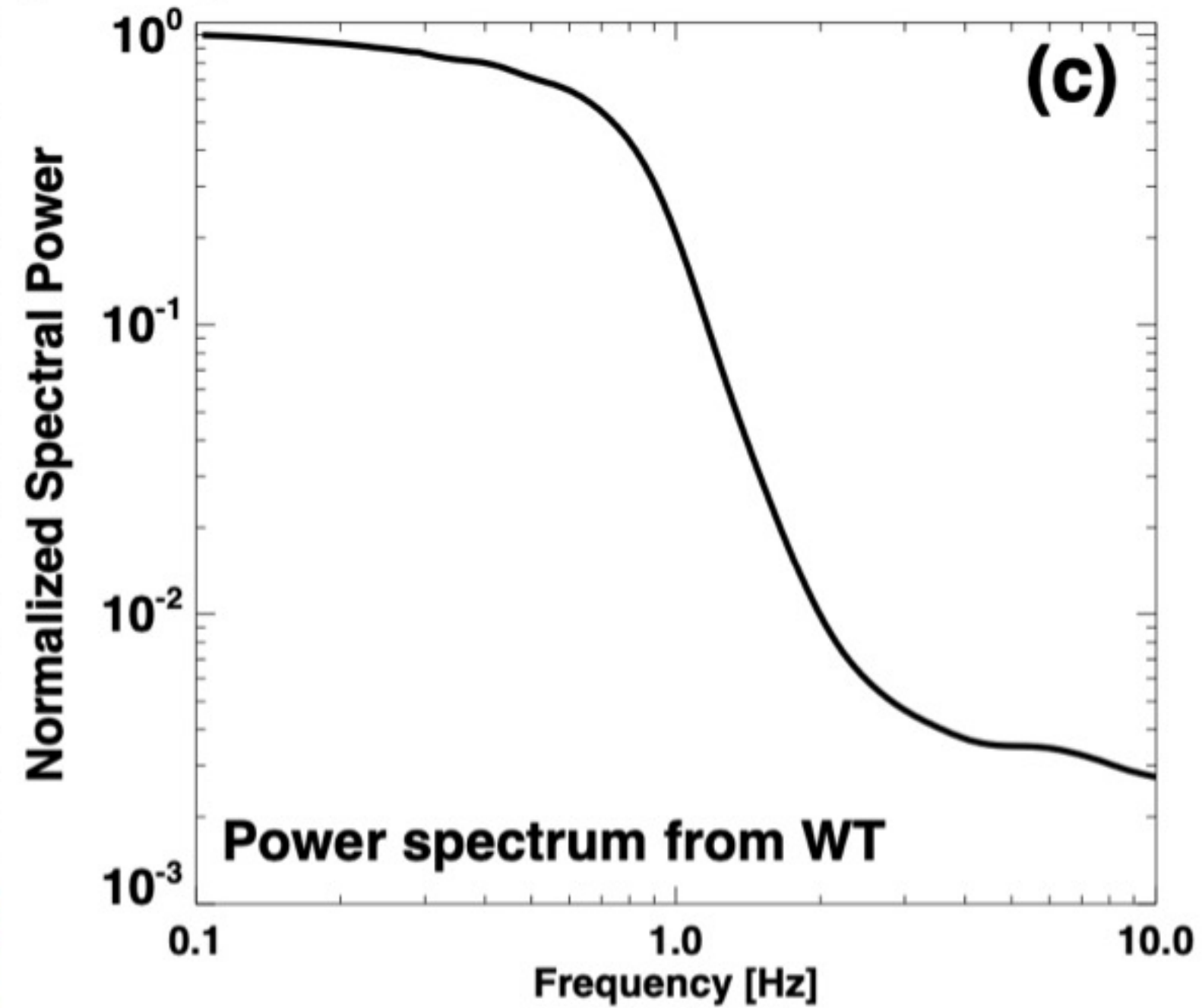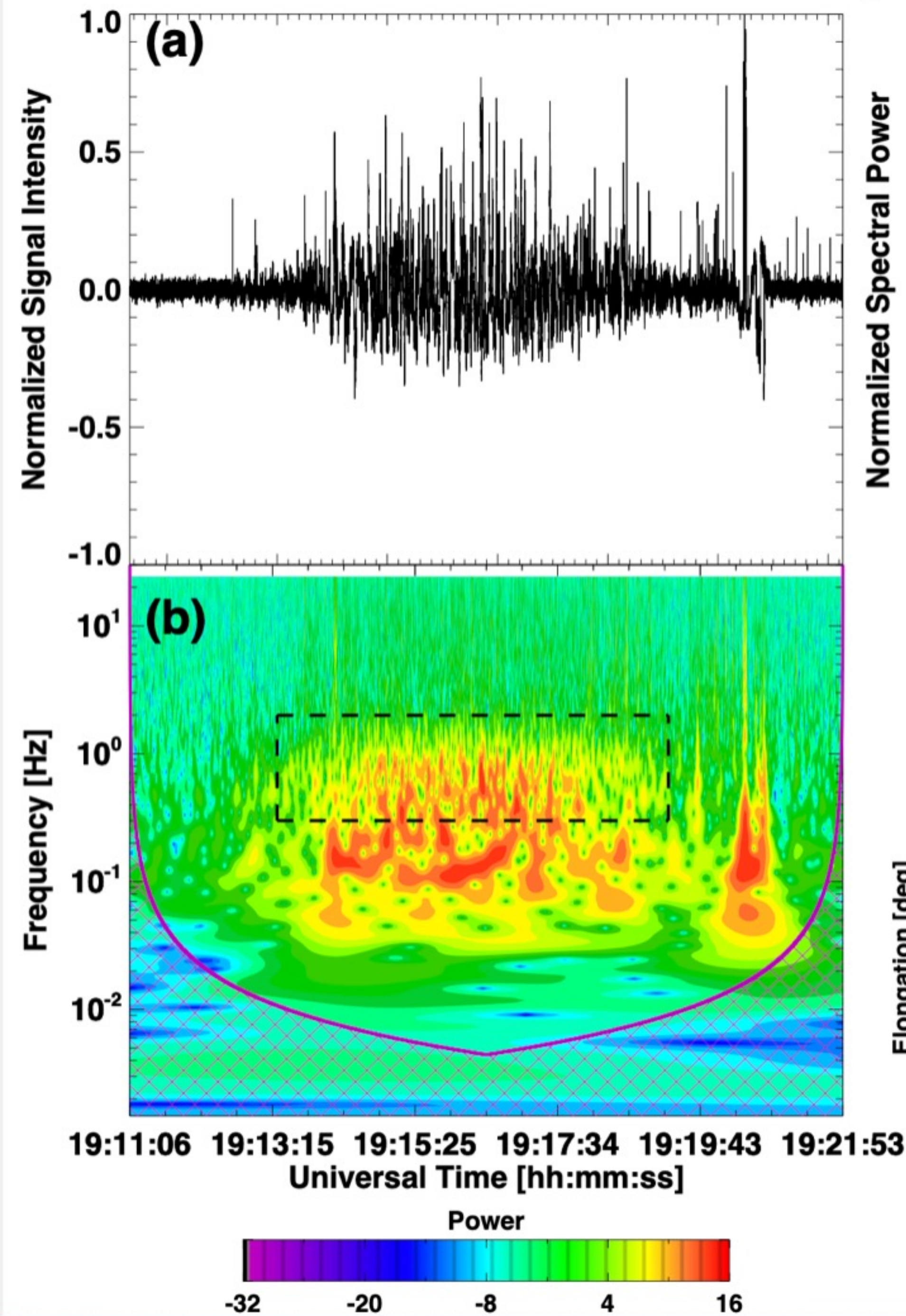**Figure 9.**

MEXART 3C48 April 8, 2021

Figure 10.